Published in final edited form as:
J Comp Neurol. 2013 June 1; 521(8): 1803–1816. doi:10.1002/cne.23260.

Basal bodies exhibit polarized positioning in zebrafish cone photoreceptors

Michelle Ramsey and **Brian D. Perkins**
Department of Biology, Texas A&M University, College Station, TX 77843

Abstract

The asymmetric positioning of basal bodies, and therefore cilia, is often critical for proper cilia function. This planar polarity is critical for motile cilia function but has not been extensively investigated for non-motile cilia or for sensory cilia such as vertebrate photoreceptors. Zebrafish photoreceptors form an organized mosaic ideal for investigating cilia positioning. We report that in the adult retina, the basal bodies of red, green-, and blue-sensitive cone photoreceptors localized asymmetrically on the cell edge nearest to the optic nerve. In contrast, no patterning was seen in the basal bodies of ultraviolet-sensitive cones or in rod photoreceptors. The asymmetric localization of basal bodies was consistent in all regions of the adult retina. Basal body patterning was unaffected in the cones of the XOPS-mCFP transgenic line, which lacks rod photoreceptors. Finally, the adult pattern was not seen in 7 day post fertilization (dpf) larvae as basal bodies were randomly distributed in all the photoreceptor subtypes. These results establish the asymmetrical localization of basal bodies in red-, green-, and blue-sensitive cones in adult zebrafish retinas but not in larvae. This pattern suggests an active cellular mechanism regulated the positioning of basal bodies after the transition to the adult mosaic and that rods do not seem to be necessary for the patterning of cone basal bodies.

Keywords

Basal body; cilia; zebrafish; polarity; retina; cones

Introduction

The light-sensitive outer segment of vertebrate photoreceptors develops from a primary cilium, which is anchored to the apical surface of the inner segment by the basal body (De Robertis, 1956; 1960). The connecting cilium also serves as the only conduit for transporting proteins involved in phototransduction from the inner segment to the outer segment. As such, defects in cilia formation or maintenance often lead to photoreceptor degeneration, a common symptom of ciliopathies (Adams et al., 2007). Anatomical studies of outer segment morphogenesis over several decades have primarily focused on cilia growth and disc membrane formation (Besharse et al., 1985; De Robertis, 1956; Knabe and Kuhn, 1997; Steinberg et al., 1980). Very little is known, however, about the initial steps leading to cilia

Corresponding author (current address): Brian Perkins, Cole Eye Institute (i31), Department of Ophthalmology, Cleveland Clinic Foundation, Cleveland, OH 44195, USA, Ph: 216-444-9683.

Conflict of interest. None.

Role of Authors
All authors had full access to all the data in the study and take responsibility for the integrity of the data and the accuracy of the data analysis. Study concept and design: MR, BP. Acquisition of data: MR. Analysis and interpretation of data: MR, BP. Drafting of the manuscript: MR, BP. Critical revision of the manuscript for important intellectual content: MR, BP. Statistical analysis: MR, BP. Obtained funding: BP. Administrative, technical, and material support: BP. Study supervision: BP.

formation in photoreceptors or subsequent changes in cilia structure during photoreceptor maturation.

One of the earliest steps in cilia formation is the migration and docking of the basal body at the apical cell surface. Once the basal body docks, it extends microtubules to form the axoneme of the cilium (Dawe et al., 2007). While recent studies have provided some insight on the molecular mechanisms governing these processes, the results often appear context-specific, or even contradictory, and no consensus model on cilia formation exists (see (Wallingford and Mitchell, 2011) for review). For example, basal body docking requires the organization of the apical actin cytoskeleton (Boisvieux-Ulrich et al., 1990), a process involving the RhoA GTPase (Pan et al., 2007). Studies of zebrafish motile cilia revealed that RhoA activation requires the forkhead box (F-box) transcription factor Foxj1 (Yu et al., 2008) and loss of Foxj1 resulted in actin cytoskeleton defects and a failure to properly dock basal bodies (Gomperts et al., 2004). While Foxj1 factors serve as “master regulators” for genes essential for motile cilia, primary (9+0) and sensory cilia are unaffected by loss of Foxj1 (Brody et al., 2000; Yu et al., 2008), indicating that other factors likely govern actin assembly and/or RhoA activation. Additional evidence suggests that basal body docking and ciliogenesis also requires planar cell polarity (PCP) signaling.

PCP refers to the ability of cells or cellular structures (e.g. cilia) to orient within a plane of a tissue and this phenomenon is controlled by the PCP signaling cascade (for recent reviews, see (Goodrich and Strutt, 2011; Gray et al., 2011; Simons and Mlodzik, 2008). Early studies in *Drosophila* elucidated a core group of proteins responsible for PCP signaling activity. The pathway includes the transmembrane proteins Van Gogh (Vangl), Flamingo (Fmi) and Frizzled (Fz) and the cytoplasmic proteins Dishevelled (Dsh), Diego (Dgo) and Prickle (Pk). This group of core proteins subsequently signals through downstream effectors, such as Inturned and Fuzzy. Subsequent analyses in *Xenopus* (Wallingford et al., 2000), zebrafish (Heisenberg et al., 2000; Jessen et al., 2002), and mice (Montcouquiol et al., 2003) demonstrated that the pathway is evolutionarily conserved in vertebrates and multiple homologs have been identified for each of these proteins (Simons and Mlodzik, 2008). Somewhat unexpectedly, PCP has now been linked to defects in cilia, although the exact nature of this relationship is not entirely clear.

In multiciliated cells of the *Xenopus* epidermis, the cytoplasmic protein Dishevelled, a core component of the PCP pathway, mediated activation of RhoA and basal bodies failed to dock in the absence of Dishevelled (Park et al., 2008). Studies in *Xenopus* and mouse also found actin cytoskeleton and cilia defects following the loss of downstream PCP effectors Inturned and Fuzzy (Gray et al., 2009; Park et al., 2006). Thus, components of the PCP pathway can function in cilia formation, but reports detailing the precise roles for specific proteins are often contradictory. For example, formation of primary cilia was not affected by the loss of the core PCP gene *vangl2* in zebrafish (Borovina et al., 2010), but basal body docking and cilia formation were perturbed by morpholino knockdown of Vangl2 in multiciliated epidermal cells of *Xenopus* (Mitchell et al., 2009). Nevertheless, following the loss of Vangl2 both motile primary cilia and motile epidermal cilia exhibited defects in planar orientation and asymmetric tilting, characteristics which are necessary to produce directional fluid flow (Borovina et al., 2010; Mitchell et al., 2009). Taken together, these results indicate that PCP components in motile cilia function in basal body docking and/or planar orientation of cilia, which coordinates cilia beating to create directional fluid flow. Current data do not suggest, however, that primary or sensory cilia universally require planar polarization across a tissue. Such cilia are non-motile and the need for ciliary polarization has not been thoroughly investigated, particularly in vertebrate photoreceptors.

In this study, we investigated planar positioning of basal bodies and cilia within zebrafish photoreceptors. The zebrafish retina is ideal for these studies because the photoreceptors are arranged into a precise, geometric lattice known as the row mosaic (Engstrom, 1960; Larison and Bremiller, 1990; Raymond et al., 1993). This mosaic provides an ideal background to identify planar polarization of individual cilia within the plane of the epithelia (Fig. 1A). Zebrafish possess four distinct cone subtypes, which we will refer to as ultraviolet (UV)-, blue-, red-, and green-sensitive cones (Branchek and Bremiller, 1984). Morphologically, the UV- and blue-sensitive cones exist as single cones, while the red- and green-sensitive cones form a double-cone pair (Branchek and Bremiller, 1984; Raymond et al., 1993). UV- and blue-sensitive cones alternate with rows of red- and green-sensitive cones (Fig. 1A). These rows radiate out from the optic nerve with the oldest cones being near the center (Allison et al., 2010). The rods are arranged in squares surrounding the UV-sensitive cones (Fadool, 2003).

Cone photoreceptors in the adult zebrafish retina are also tiered within the photoreceptor layer. UV-sensitive cones are located most vitreally and are followed (moving in the scleral direction) by blue-sensitive cones and red-/green-sensitive double cones (Branchek and Bremiller, 1984; Raymond et al., 1993). This vertical tiering dramatically separates the ellipsoids and outer segments of different cone types. The ellipsoids and outer segments of UV-sensitive cones lie below the ellipsoid region of blue-sensitive cones, while the blue-sensitive cone outer segments terminate near the base of the double-cone outer segments. This tiering predicts a similar tiering of the basal bodies in photoreceptors, which anchor the connecting cilia to the apical surface of the inner segments (Fig. 1A). As each cell's identity in relation to the surrounding cells is easily identified, based on both the mosaic pattern and the tiering of the cone subtypes, the zebrafish photoreceptor mosaic is an excellent system to search for planar polarization of basal bodies.

Larval zebrafish lack the highly patterned row mosaic of cone photoreceptors seen in adults, but they do exhibit a non-random mosaic array of cones (Allison et al., 2010). A transition occurs between 20–36 days post fertilization (dpf), whereby cones born after this time are arranged in the adult row mosaic. Cones generated during embryonic and larval stages remain as a distinct larval remnant surrounding the optic nerve in the adult retina. As the adult retina grows, new cones are produced at the margins and adopt the row mosaic. We have identified a pattern of basal body positioning in zebrafish red-, green-, and blue-sensitive cones. At the apical surface of the inner segment of these cones, the basal bodies are positioned asymmetrically on the cell edge nearest to the optic nerve. This pattern is seen throughout the adult mosaic. In contrast, the basal bodies of UV-sensitive cones and rods are not patterned. In 7 day-old larval retinas no pattern is evident. We also report that in a transgenic line that undergoes early degeneration of rod photoreceptors, no change in the patterning of cone basal bodies was observed, suggesting that rods are not necessary for establishing the pattern of the cone basal bodies.

Methods

Zebrafish care and maintenance

Zebrafish (*Danio rerio*) were maintained according to standard procedures (Westerfield, 1995). Light-adapted wild-type AB/Ekkwill hybrids, *Tg(Ta1C:GFP)* (Kennedy et al., 2007), and *Tg(-5actb2:cetn2-GFP)cu6* (Randlett et al., 2011) fish were used for quantification of wild-type cone basal body positioning. Dark-adapted *Tg(XlRho:EGFP)fl1* fish (referred to here as XOPS-GFP) utilize the *Xenopus* opsin promoter to drive GFP in rod photoreceptors and were used to analyze rod basal bodies (Fadool, 2003). The *Tg(XlRho:gap43-CFP)* transgenic line, which is referred to here as XOPS-mCFP, expresses a membrane-targeted

cyan fluorescent protein (CFP) in rod photoreceptors that causes degeneration of rods without affecting cones (Morris et al., 2005).

Immunohistochemistry and imaging

Adult light-adapted fish were sacrificed, and their eyes were enucleated. The retinas were removed and 4–5 incisions were made so that they could subsequently be laid flat. The retinas were fixed 3 hours to overnight (ON) in 4% paraformaldehyde in phosphate buffered solution (PBS: 137 mM NaCl, 2.7 mM KCl, 10 mM Na_2HPO_4, 1.76 mM KH_2PO_4, pH 7.4) at 4°C. Alternatively, dark-adapted fish were sacrificed and their heads were fixed ON as above. After fixation, their eyes were enucleated, and their retinas were prepared as above. Retinas were infiltrated with 30% sucrose in PBS at 4 °C until they had sunk and with tissue freezing medium (TFM; Triangle Biomedical Sciences, Durham, N.C.) at room temperature for 20 minutes. Retinas were flat-mounted in TFM between two coverslips spaced with #1 coverslips prior to freezing. The flat-mounted retinas were cryosectioned such that each tangential section (10 μm) was slightly oblique and off-parallel to the outer limiting membrane. Cryosections were mounted on gelatin-coated slides and dried overnight at room temperature. The sections were rehydrated and washed in 0.1% TWEEN 20 and 0.1% DMSO in PBS (PBSTD). To detect γ-tubulin in the basal bodies, sodium citrate antigen retrieval (adapted from (Jiao et al., 1999) was performed by maintaining slides at 70–90°C for 30 min in while submerged in 10 mM sodium citrate. The slides were cooled at RT while submerged in sodium citrate solution. Slides were blocked 1–2 hours at RT in 5% normal goat serum in PBSTD and incubated overnight at 4°C in primary antibody diluted in blocking solution. After washing in PBSTD, slides were incubated 1 hour at room temperature in the appropriate AlexaFluor secondary antibodies (Invitrogen, 1:500) and in the fluorescent nuclear stain 4,6-diamidino-2-phenlindole dihydrochloride (DAPI, Invitrogen, Eugene, OR; 1:10,000). Larval zebrafish (7 dpf) were prepared as described for adult retinas, except that sodium citrate antigen retrieval was not used. Sagittal sections of whole larvae were taken, and photoreceptors perpendicular to the visible optical plane were analyzed.

Antibody Characterization

Antibodies used in this study are summarized in Table 1. The mouse monoclonal anti-γ-tubulin antibody (Sigma-Aldrich, T6557; mouse IgG1 isotype) is a well-established marker for basal bodies. The antibody was raised against a synthetic γ-tubulin peptide (N-terminal amino acids 38-53) conjugated to KLH and was derived from the GTU-88 hybridoma produced by the fusion of mouse myeloma cells and splenocytes from an immunized mouse. It recognizes a 48 kDa epitope located in the N-terminal amino acids 38-53 of γ-tubulin (manufacturer's data sheet).

The rabbit polyclonal anti-GFP antibody (Invitrogen, A-111-22, IgG isotype) was raised against Green Fluorescence Protein isolated directly from the jellyfish *Aequorea victoria* and the IgG fraction purified by ion-exchange chromatography (manufacturer's data sheet). This antibody was used to identify the centrin-GFP fusion protein as well as eGFP in the XOPS-GFP line. In centrin-GFP transgenic animals, staining with this antibody gave an identical pattern to that of anti-γ-tubulin, another marker for basal bodies. Furthermore, no staining was observed when the antibody was used to stain tissue from zebrafish lacking the centrin-GFP transgene.

Rabbit polyclonal antibodies against the zebrafish opsin proteins were a generous gift of Dr. David Hyde (University of Notre Dame). A carboxyl terminal polypeptide generated from the amplified cDNA template for zebrafish green opsin (5′-GAATTCAGCTTTGCTGCCTGGATCTTCT-3′ and 5′-

CTCGAGCAGATCTATGCAGGGAACAGAGGA-3′) was used to generate polyclonal antibodies against zebrafish green opsin. Amino terminal polypeptides were generated from the amplified cDNA templates for zebrafish blue opsin (5′-GAATTCGAAGCAACAACAGCAAACGC-3′ and 5′-CTCGAGGGTAAGAACGTTGATGGCAG-3′) and ultraviolet opsin (5′-GAATTCGCGTGGGCCGTTCAATT-3′ and 5′-CTCGAGTTCATCGTGACGAAGAGGACG-3′) to generate polyclonal antibodies against the zebrafish blue and ultraviolet opsins, respectively. All antibodies detected single bands that were near the expected sizes of the individual opsin proteins (~38 kDa) and labeled the outer segments of the appropriate cone subtypes (Vihtelic et al., 1999).

The mouse monoclonal antibody Zpr-1 (Fret-43; Zebrafish International Resource Center, Eugene, OR) recognizes the arrestin 3-like (*arr3l*) protein in the red/green-sensitive double cones (Ile et al., 2010). The Zpr-1 antibody recognized a single 45-kDa protein in Western blots of zebrafish retinal lysates and was confirmed as arrestin 3-like by MALDI-TOF mass spectrometry analysis and by loss of Zpr-1 immunofluorescence in *arr3l* morphant retinas (Ile et al., 2010). Stained cells were identified as red-/green-sensitive double cones on the basis of anatomical location and morphological features such as outer segments and synaptic terminals (Larison and Bremiller, 1990).

The mouse monoclonal antibody 4C12 was a gift from Dr. James Fadool (Florida State University) and was generated by immunizing mice with homogenized zebrafish retinal extracts (Fadool, 1999). Hybridomas were screened for antibodies that labeled the zebrafish retina and 4C12 specifically recognized cells within the outer nuclear layer. Based on the morphology of the outer segments and the tiering within the outer nuclear layer, 4C12 labels an uncharacterized epitope on rod photoreceptors. Additional evidence that 4C12 labels rods is that only 4C12 staining of regenerating rod photoreceptors is seen in the rod degeneration XOPS-mCFP line and the increase in 4C12 staining in *tbx2b* mutants, which show increased numbers of rod photoreceptors (Alvarez-Delfin et al., 2009; Morris et al., 2005).

Sections were imaged by taking z-stacks of approximately 12–20 optical sections at 0.5–0.8 μm steps with a Zeiss ImagerZ1 fluorescence microscope with an ApoTome. The location of each field in relation to the optic nerve (near the optic nerve, in the middle of the retina, or in the peripheral retina) was recorded when each field was imaged. The larval remnant was identified by the lack of the organized adult cone mosaic in cells nearest to the optic nerve. To define the other areas of the retina, the radius of the retina was visually divided into thirds, the first starting immediately outside the larval remnant and the third ending at the retinal margin (Fig. 4E). Fields that were very close to the boundaries between the different regions were not analyzed. All images shown consist of either a single plane or multiple optical sections from one z-stack obtained using AxioVision or ZEN (blue edition) (v. 4.8.2 or v. 1.0.0.0, respectively, Zeiss). The RGB and CMYK levels of fully assembled figures were adjusted using Adobe Photoshop.

Quantification of basal body localization

Basal body positions were determined from images of adult retinas stained with γ-tubulin as described above. Each optical section of the z-stack was analyzed individually, and all data for a given cone subtype within a z-stack was combined to form one data set. Each data set contains the positions of basal bodies from red-/green-sensitive cones, blue-sensitive cones, UV-sensitive cones, or rods within one z-stack. Each basal body was located along the periphery of the apical side of the inner segment and the angular position was quantified using AxioVision or ZEN. As rows of cells radiate outward from the optic nerve ((Allison et al., 2010); Fig. 1A), the angular position of a basal body was defined by the direction of the row within the field relative to the optic nerve (Fig. 1B). The direction of the optic nerve

was arbitrarily defined as an angular vector of 90° (Fig. 1B). All subsequent calculations and graphs were completed using Excel (Microsoft, 2010) using standard statistical methods (Batschelet, 1981; Fisher, 1993; Zar, 1996). Formulas, when possible, were confirmed using StatistiXL (v. 1.8). The angular positions of all the basal bodies from one data set were plotted around a unit circle with the point (1,0) corresponding with 0°. The Rayleigh test was used to determine the probability that the mean position represented a true mean position of the population. We calculated the circular 95% confidence interval for the mean position of each data set. To calculate the mean position of multiple data sets (i.e. the grant mean position) and the corresponding 95% confidence internal, all data sets to be combined were represented by their mean vectors and the angular position of the grand mean vector was calculated. The circular 95% confidence intervals for the grand mean position were calculated as for a second-order mean angle (Zar, 1996). If the strength of the trend was very weak, then no circular confidence interval could be calculated. Finally, positions from red- and green-sensitive cones were combined because the double cones and their basal bodies are found at very similar depths in the retina.

Results

To analyze the positioning of basal bodies in zebrafish photoreceptors, we labeled cryosections of flat-mounted adult retinas with γ-tubulin, a specific marker for basal bodies (Stearns et al., 1991). We hypothesized that if an active signaling mechanism controlled cilia positioning in photoreceptors, then the basal bodies within a plane of cells would align in a reproducible pattern, which would be propagated within each subtype (Fig. 1C, D). Alternatively, in the absence of an active signaling mechanism, basal bodies would be distributed randomly on the apical surface of the inner segment of the photoreceptors (Fig. 1E). In either scenario, the photoreceptor positioning within the mosaic remains unaffected. We first identified individual cell types by their vertical tiering position within the outer nuclear layer, their position within the row mosaic, and by staining with individual opsin antibodies to label outer segments (Figure 2).

Within the adult row mosaic, basal bodies of the red-, green-, and blue-sensitive cones appear to be located at the same position along the periphery of most cells within a single field (Fig. 3A, B, D, E). The angular positions of basal bodies within a single field of cells were combined into a unique data set. Each data set was then quantified in relation to the direction of the optic nerve and graphed on a circular plot (Fig. 3G, H). The position of the optic nerve was determined from low-magnification views of the field of cells and from the orientation of cell rows. Red- and green-sensitive cones form a double cone pair and the basal bodies within each pair appeared to be similarly aligned. As such, the angular positions reflect the combined data from both subtypes. Within individual data sets, basal bodies of the red-/green-sensitive cones exhibited a strong polarization toward the optic nerve (Fig. 3G, Table 2). Basal bodies of the blue-sensitive cones also aligned preferentially on the leading edge with a low angular deviation (Fig. 3H, Table 2). The mean angular position for all basal bodies within a data set was calculated and graphed as the mean vector (Fig. 3G, H; black arrows). The length of this vector corresponds to the strength of the trend. In contrast to the other cone subtypes, the basal bodies of UV-sensitive cones appeared randomly distributed around the edge at the apical inner segment (Fig. 3C, F, I).

For each cone subtype, the mean angular positions of basal bodies from several data sets were graphed on circular plots and used to calculate a grand mean angular position (Fig. 4A–D; Table 2). The basal bodies of the red-/green-sensitive double cones and blue-sensitive cones were strongly polarized toward the optic nerve in almost all fields, although a few data sets were less polarized. The grand mean angular position of all basal bodies in the red/green-sensitive cones and the blue-sensitive cones was 91o and 87°, respectively,

while that of the UV-sensitive cones was 151° (Fig. 4D). As cone organization transitions into the row mosaic during metamorphosis (Allison et al., 2010), which is a time of significant morphological and hormonal changes (Brown, 1997; Parichy et al., 2009), we next addressed whether basal body patterning may be influenced by developmental changes. Basal body positioning was analyzed in multiple fields near the optic nerve, near the middle of the retina, and near the peripheral retina (Fig. 4E; see Methods for details). For the red-/green-sensitive cones and the blue-sensitive cones, no deviation existed in the average angular position of basal bodies in various regions of the retina (Fig. 4F; Table 2). The mean angular position of basal bodies for the UV-sensitive cones remained highly variable across the adult retina. Taken together, these results show that in the adult retina basal bodies of the blue-sensitive cones and the red-/green-sensitive double cones strongly polarize toward the optic nerve while basal bodies of the UV-sensitive cones do not organize in a polarized fashion.

We next asked whether basal bodies in adult rod photoreceptors were polarized. Although cone subtypes are tiered within the outer nuclear layer (ONL), the cell bodies and ellipsoids remain in close proximity to each other (Fig. 1A). In contrast, the rod nuclei and cell bodies are located on the most vitreal portion of the ONL while the slender rod inner segments project past the cones such that the rod ellipsoids and outer segments cluster above the cone outer segments. To clearly follow rods from the cell body to the ellipsoid, we used the *Tg(XlRho:EGFP)*^{fl1} transgenic line, which expresses a soluble eGFP throughout the rods, but not in cones (Fadool, 2003). Tangential cryosections were stained with antibodies against γ-tubulin and GFP to label basal bodies within the rods. Rod basal bodies were identified in cells immunopositive for GFP (Fig. 5A). Although the transgene expresses a soluble GFP that extends throughout the cytoplasm, the GFP immunoreactivity was limited to the periphery of the rods (Fig. 5A). This may reflect reduced antigen accessibility due to the sodium citrate treatment required to label with γ-tubulin or by the exclusion of GFP from the mitochondria within the ellipsoids (Fadool, 2003). Similar to the UV-sensitive cones, rod basal bodies were randomly oriented in all fields analyzed (Fig. 5B, C)

The random positioning of basal bodies in the UV-sensitive cones suggests that the mechanisms guiding basal body polarization in the other cone subtypes are missing from UV-sensitive cones or that a non-permissive signal from neighboring cells may be present. As the cell bodies of UV-sensitive cones largely contact only rods, we asked if the absence of rods would permit the polarized organization of basal bodies with the UV-sensitive cones. Toward this end, we analyzed basal body positioning in cones from the XOPS-mCFP transgenic line (Morris et al., 2005). This line expresses a membrane-targeted cyan fluorescence protein (CFP) that selectively kills rods beginning at 3.5 dpf, with an almost complete absence of rods by 5 dpf (Morris et al., 2005). The adults completely lack rods outside the retinal margin (Morris et al., 2005). We did not detect any effects of rod degeneration on the cone row mosaic and individual subtypes were located in the normal tiering patterns. As in wild-type retinas, we found that the basal bodies of red-/green- and blue-sensitive cones in the adult XOPS-mCFP mosaic remained strongly oriented towards the optic nerve while UV-sensitive cones had randomly oriented basal bodies (Fig. 6, Table 2). The average angular positions of the red-/green-sensitive cones and blue-sensitive cones were 81° and 88°, respectively. There appeared to be more deviation in basal body positioning in the red-/green-sensitive cones of XOPS-mCFP fish than in wild-type adults, but the overall trend remained non-random (Table 2). In contrast, the basal bodies of UV-sensitive cones remained randomly positioned. These results suggest that rod photoreceptors do not negatively affect the arrangement of basal bodies in UV-sensitive cones. Furthermore, rod degeneration in XOPS-mCFP transgenic zebrafish does not dramatically alter the intrinsic pattern observed in red-/green-sensitive and blue-sensitive cones.

We next asked if the basal body position we observed also appeared in the larval retina. Unlike the adult retina, the larval retina lacks the crystalline row mosaic, which prevents identification of cone sub-types simply by position within the mosaic (Allison et al., 2010). We therefore analyzed sagittal sections of 7 dpf wild-type zebrafish retinas labeled with polyclonal antibodies against cone opsins, which label outer segments, and with monoclonal antibodies that label entire red-/green-sensitive cones and rods. We also used the *Tg(-5actb2:cetn2-GFP)*^{cu6} line in order to identify basal bodies with a centrin-GFP transgene (Randlett et al., 2011). Centrins are Ca^{2+} binding proteins that localize to basal bodies (Wolfrum, 1995) and the centrin-GFP transgene is a viable marker for centrioles and basal bodies(Borovina et al., 2010). Basal body position was quantified using the *Tg(-5actb2:cetn2-GFP)*^{cu6} line and the results were similar to that obtained from immunostaining with γ-tubulin (Figure 7). Transgenic larvae were analyzed at 7 days post fertilization (dpf) when photoreceptor outer segments were present and the animals exhibit robust visual behaviors (Brockerhoff et al., 1995). Unlike the adult retina, the larval retina lacks the crystalline row mosaic, which prevents identification of cone sub-types simply by position within the mosaic (Allison et al., 2010). We therefore analyzed sagittal sections of 7 dpf wild-type zebrafish retinas labeled with polyclonal antibodies against cone opsins, which label outer segments, and with monoclonal antibodies that label entire red-/green-sensitive cones and rods. Serial sections could then be labeled with GFP antibodies to identify centrin-GFP. Fields of cells that contained the optic nerve also contained photoreceptors that were perpendicular to the optical plane of the image and could be viewed head-on as in a flat-mounted retina. The basal bodies of red-/green- and blue-sensitive cones were located at similar optical depths within the retina, while the basal bodies of the UV-sensitive cones were located more vitreally. Consistent with previous reports (Vihtelic et al., 1999), zpr-1 co-labeled the cones labeled with anti-green opsin and did not co-localize with the cones labeled with anti-blue opsin (Figure 2). Basal bodies located within zpr-1 positive red-/green-sensitive cones were randomly positioned (Fig. 8C, G). To accurately identify blue-sensitive cones, we immunostained larval sections with both the monoclonal zpr-1, which labels red-/green-sensitive cones, and the rod-specific monoclonal antibody 4C12 (Morris et al., 2005). Basal bodies in cones lacking both zpr-1 and 4C12 staining (i.e. blue-sensitive) were also randomly positioned (Fig. 8D, H). The UV-sensitive cones, which did not stain with zpr-1 and could be identified as having wide outer segments and by their vitreally tiered position within the ONL, also possessed randomly positioned basal bodies (Fig. 8E, I). Rods were identified by staining sections with only 4C12 and the basal bodies within 4C12-positive cells were also randomly positioned (Fig. 8F, J). Taken together, these results show that basal bodies and cilia do not polarize in larval animals, suggesting an active mechanism that rearranges cilia polarity after photoreceptor outer segments have formed.

Discussion

In this study, we present the identification and initial description of the planar polarization of basal bodies within adult zebrafish photoreceptors. The data show for the first time that basal bodies of red-/green-sensitive and blue-sensitive cones preferentially align on the edge of the ellipsoid directed towards the optic nerve. UV-sensitive cones and rod photoreceptors do not, however, exhibit this polarized positioning. Furthermore, as this pattern does not exist in the larval retina, the mechanism(s) driving this polarization do not occur during photoreceptor differentiation. Finally, basal body positioning within the cones was not disrupted by early-onset rod degeneration. As basal bodies anchor the cilium within the cell body, we conclude that cilia positioning within specific cone subtypes become asymmetrically positioned in an age-dependent manner.

Planar polarization of basal bodies and cilia has been described for multiciliated cells, as well as primary motile cilia of the embryonic node (Borovina et al., 2010; Mirzadeh et al., 2010; Mitchell et al., 2009; Park et al., 2008), but the polarization of non-motile cilia and sensory cilia remains poorly understood. The asymmetric localization of cilia to one side of the apical cell surface has been termed “translational planar polarity” (Mirzadeh et al., 2010), and is observed for ependymal cilia (Mirzadeh et al., 2010), kinocilia of the vertebrate inner ear (Jones et al., 2008) and in lens fiber cells (Sugiyama et al., 2010). Such non-random arrangements clearly argue for active signaling mechanism(s) to regulate basal body placement. However, while components of the PCP pathway govern the planar polarization of basal bodies in both motile and non-motile cilia, reports differ on whether an intact PCP pathway is necessary (see (Wallingford and Mitchell, 2011) for review). For motile cilia, planar polarization of basal bodies coordinates the beating by multiple cilia on a single cell, as well as coordinating ciliary beating across a plane of cells (Wallingford, 2010). In contrast, it is not immediately obvious why the non-motile cilia of photoreceptors would require polarized positioning. Photoreceptor packing should not depend on cilia position, since the diameter of the cilium is considerably smaller than that of the outer segment and cilia placement would not influence outer segment location. Consistent with this, the placement of UV-sensitive cones and rods into the photoreceptor mosaic occurs without cilia adopting any translational polarity. In a similar fashion, the loss of PCP signaling disrupted the hexagonal cell packing of lens fiber cells, but the planar polarization of primary cilia was unaffected. This suggests that translational polarity of cilia and cellular packing are independent, at least in some cell types (Sugiyama et al., 2010).

Why do the basal bodies exhibit translational polarity in red-/green-sensitive and blue-sensitive cones, but not in the UV-sensitive cones and rods? One possibility is basal body positioning is a cone-specific phenomenon. The UV-sensitive cones and rods share a number of similarities not shared by other cones. It has been suggested that rods and UV-sensitive cones, the likely S-cone homolog, share a common multipotent progenitor in teleosts (Alvarez-Delfin et al., 2009) and this may skew UV-sensitive photoreceptors into a more “rod-like” cell. The lack of planar polarity in rod basal bodies could explain why this phenomenon was not observed earlier as the rod-dominated mouse retina remains the favored model of study. It is important to note, however, that an examination of adult retinas from the cone-dominated tree shrew, *Tupaia*, found that cilia were “located eccentrically on the same side of the inner segments in hundreds of neighbouring cones…” but such a phenomenon was rarely seen in younger animals (Knabe and Kuhn, 1998). An alternative, though not mutually exclusive explanation is that the signaling mechanism required to position the basal bodies must operate through specific contacts at the level of the myoid or ellipsoid. The ellipsoids of the UV-cones are located below those of the other cones, while rod ellipsoids are more scleral than the other cones. Thus, neither the UV-sensitive cones nor the rods make contact with other cells at the level of the ellipsoids to propagate a signal (Fig. 1A). The lack of cell-cell contact between ellipsoids would likely prevent any kind of planar signaling from neighboring cones to the UV-cones, and even rods. This may also explain why basal bodies in UV-sensitive cones failed to polarize in the XOPS-mCFP line, as the absence of rods does not affect the ellipsoid position of UV-sensitive cones and the ability of these cells to receive a polarizing signal.

It is interesting to note that basal bodies become polarized after the larval stage, likely during the metamorphic changes into adulthood. This suggests that the mechanisms governing basal body polarization are not required for photoreceptor development but may serve critical functions later in photoreceptor maturation or maintenance. The lack of an observable basal body pattern in larvae precludes the analysis of most zebrafish mutants to search for candidate signaling pathways, as these mutants are typically lethal prior to metamorphosis. Creating genetically mosaic animals by blastula transplantation (Moens and

Fritz, 1999) may allow examination of cells lacking key genes, as long as these genes are not essential for photoreceptor differentiation. Previous studies have noted that the larval mosaic also transitions into the adult row mosaic at metamorphosis and may reflect a change in visually mediated behaviors such as feeding and mating (Allison et al., 2010). It is unclear if basal body polarization simply correlates temporally with this anatomical rearrangement or if these processes share similar molecular mechanisms.

In summary, we provide the first detailed evidence that basal bodies in vertebrate photoreceptors show planar polarity. A similar phenomenon was briefly mentioned for tree shrews (Knabe and Kuhn, 1998), suggesting that basal body polarity can also occur in mammals, including primate-like animals. Such planar polarity is critical for motile cilia function but the importance for primary cilia and sensory cilia is unknown.

Acknowledgments

We are very grateful to James Fadool and his lab for assistance with observing the photoreceptor mosaic. We also thank James Fadool, Sue Brockerhoff, David Hyde, Ann Morris, and Brian Link for the gifts of animals and reagents. Support is from NIH Grant EY017037.

References

Adams NA, Awadein A, Toma HS. The retinal ciliopathies. Ophthalmic Genet. 2007; 28(3):113–125. [PubMed: 17896309]

Allison WT, Barthel LK, Skebo KM, Takechi M, Kawamura S, Raymond PA. Ontogeny of cone photoreceptor mosaics in zebrafish. J Comp Neurol. 2010; 518(20):4182–4195. [PubMed: 20878782]

Alvarez-Delfin K, Morris AC, Snelson CD, Gamse JT, Gupta T, Marlow FL, Mullins MC, Burgess HA, Granato M, Fadool JM. Tbx2b is required for ultraviolet photoreceptor cell specification during zebrafish retinal development. Proc Natl Acad Sci U S A. 2009; 106(6):2023–2028. [PubMed: 19179291]

Batschelet, E. Circular statistics in biology. Vol. xvi. London ; New York: Academic Press; 1981. p. 371

Besharse JC, Forestner DM, Defoe DM. Membrane assembly in retinal photoreceptors. III. Distinct membrane domains of the connecting cilium of developing rods. J Neurosci. 1985; 5(4):1035–1048. [PubMed: 3156973]

Boisvieux-Ulrich E, Laine MC, Sandoz D. Cytochalasin D inhibits basal body migration and ciliary elongation in quail oviduct epithelium. Cell Tissue Res. 1990; 259(3):443–454. [PubMed: 2317839]

Borovina A, Superina S, Voskas D, Ciruna B. Vangl2 directs the posterior tilting and asymmetric localization of motile primary cilia. Nat Cell Biol. 2010; 12(4):407–412. [PubMed: 20305649]

Branchek T, Bremiller R. The development of photoreceptors in the zebrafish, Brachydanio rerio. I. Structure. J Comp Neurol. 1984; 224(1):107–115. [PubMed: 6715574]

Brockerhoff SE, Hurley JB, Janssen-Bienhold U, Neuhauss SC, Driever W, Dowling JE. A behavioral screen for isolating zebrafish mutants with visual system defects. Proc Natl Acad Sci U S A. 1995; 92(23):10545–10549. [PubMed: 7479837]

Brody SL, Yan XH, Wuerffel MK, Song SK, Shapiro SD. Ciliogenesis and left-right axis defects in forkhead factor HFH-4-null mice. Am J Respir Cell Mol Biol. 2000; 23(1):45–51. [PubMed: 10873152]

Brown DD. The role of thyroid hormone in zebrafish and axolotl development. Proc Natl Acad Sci U S A. 1997; 94(24):13011–13016. [PubMed: 9371791]

Dawe HR, Farr H, Gull K. Centriole/basal body morphogenesis and migration during ciliogenesis in animal cells. J Cell Sci. 2007; 120(Pt 1):7–15. [PubMed: 17182899]

De Robertis E. Morphogenesis of the Retinal Rods. J Biophysic and Biocehm Cytol. 1956; 2(4 Suppl): 209–218.

De Robertis E. Some observations on the ultrastructure and morphogenesis of photoreceptors. J Gen Physiol. 1960; 43(6 Suppl):1–13. [PubMed: 13814989]

Engstrom K. Cone types and cone arrangements in retina of some cyprinids. Acta Zool (Stockholm). 1960; 41:277–295.

Fadool JM. Development of a rod photoreceptor mosaic revealed in transgenic zebrafish. Dev Biol. 2003; 258(2):277–290. [PubMed: 12798288]

Fadool JM, Fadool DA, Moore JC, Linser PJ. Characterization of monoclonal antibodies against zebrafish retina. Invest Opth Vis Sci Suppl. 1999; 40:1251.

Fisher, NI. Statistical analysis of circular data. Vol. xviii. Cambridge England ; New York, NY, USA: Cambridge University Press; 1993. p. 277

Gomperts BN, Gong-Cooper X, Hackett BP. Foxj1 regulates basal body anchoring to the cytoskeleton of ciliated pulmonary epithelial cells. J Cell Sci. 2004; 117(Pt 8):1329–1337. [PubMed: 14996907]

Goodrich LV, Strutt D. Principles of planar polarity in animal development. Development. 2011; 138(10):1877–1892. [PubMed: 21521735]

Gray RS, Abitua PB, Wlodarczyk BJ, Szabo-Rogers HL, Blanchard O, Lee I, Weiss GS, Liu KJ, Marcotte EM, Wallingford JB, Finnell RH. The planar cell polarity effector Fuz is essential for targeted membrane trafficking, ciliogenesis and mouse embryonic development. Nat Cell Biol. 2009; 11(10):1225–1232. [PubMed: 19767740]

Gray RS, Roszko I, Solnica-Krezel L. Planar cell polarity: coordinating morphogenetic cell behaviors with embryonic polarity. Dev Cell. 2011; 21(1):120–133. [PubMed: 21763613]

Heisenberg CP, Tada M, Rauch GJ, Saude L, Concha ML, Geisler R, Stemple DL, Smith JC, Wilson SW. Silberblick/Wnt11 mediates convergent extension movements during zebrafish gastrulation. Nature. 2000; 405(6782):76–81. [PubMed: 10811221]

Ile KE, Kassen S, Cao C, Vihtehlic T, Shah SD, Mousley CJ, Alb JG Jr, Huijbregts RP, Stearns GW, Brockerhoff SE, Hyde DR, Bankaitis VA. Zebrafish class 1 phosphatidylinositol transfer proteins: PITPbeta and double cone cell outer segment integrity in retina. Traffic. 2010; 11(9):1151–1167. [PubMed: 20545905]

Jessen JR, Topczewski J, Bingham S, Sepich DS, Marlow F, Chandrasekhar A, Solnica-Krezel L. Zebrafish trilobite identifies new roles for Strabismus in gastrulation and neuronal movements. Nat Cell Biol. 2002; 4(8):610–615. [PubMed: 12105418]

Jiao Y, Sun Z, Lee T, Fusco FR, Kimble TD, Meade CA, Cuthbertson S, Reiner A. A simple and sensitive antigen retrieval method for free-floating and slide-mounted tissue sections. J Neurosci Methods. 1999; 93(2):149–162. [PubMed: 10634500]

Jones C, Roper VC, Foucher I, Qian D, Banizs B, Petit C, Yoder BK, Chen P. Ciliary proteins link basal body polarization to planar cell polarity regulation. Nat Genet. 2008; 40(1):69–77. [PubMed: 18066062]

Kennedy BN, Alvarez Y, Brockerhoff SE, Stearns GW, Sapetto-Rebow B, Taylor MR, Hurley JB. Identification of a zebrafish cone photoreceptor-specific promoter and genetic rescue of achromatopsia in the nof mutant. Invest Ophthalmol Vis Sci. 2007; 48(2):522–529. [PubMed: 17251445]

Knabe W, Kuhn H. Disk formation in retinal cones of Tupaia belangeri (Scandentia). Cell Tissue Res. 1998; 292(1):67–76. [PubMed: 9506913]

Knabe W, Kuhn HJ. Ciliogenesis in photoreceptor cells of the tree shrew retina. Anat Embryol (Berl). 1997; 196(2):123–131. [PubMed: 9278157]

Larison KD, Bremiller R. Early onset of phenotype and cell patterning in the embryonic zebrafish retina. Development. 1990; 109(3):567–576. [PubMed: 2401210]

Mirzadeh Z, Han YG, Soriano-Navarro M, Garcia-Verdugo JM, Alvarez-Buylla A. Cilia organize ependymal planar polarity. J Neurosci. 2010; 30(7):2600–2610. [PubMed: 20164345]

Mitchell B, Stubbs JL, Huisman F, Taborek P, Yu C, Kintner C. The PCP pathway instructs the planar orientation of ciliated cells in the Xenopus larval skin. Curr Biol. 2009; 19(11):924–929. [PubMed: 19427216]

Moens CB, Fritz A. Techniques in neural development. Methods Cell Biol. 1999; 59:253–272. [PubMed: 9891364]

Montcouquiol M, Rachel RA, Lanford PJ, Copeland NG, Jenkins NA, Kelley MW. Identification of Vangl2 and Scrb1 as planar polarity genes in mammals. Nature. 2003; 423(6936):173–177. [PubMed: 12724779]

Morris AC, Schroeter EH, Bilotta J, Wong RO, Fadool JM. Cone survival despite rod degeneration in XOPS-mCFP transgenic zebrafish. Invest Ophthalmol Vis Sci. 2005; 46(12):4762–4771. [PubMed: 16303977]

Pan J, You Y, Huang T, Brody SL. RhoA-mediated apical actin enrichment is required for ciliogenesis and promoted by Foxj1. J Cell Sci. 2007; 120(Pt 11):1868–1876. [PubMed: 17488776]

Parichy DM, Elizondo MR, Mills MG, Gordon TN, Engeszer RE. Normal table of postembryonic zebrafish development: staging by externally visible anatomy of the living fish. Dev Dyn. 2009; 238(12):2975–3015. [PubMed: 19891001]

Park TJ, Haigo SL, Wallingford JB. Ciliogenesis defects in embryos lacking inturned or fuzzy function are associated with failure of planar cell polarity and Hedgehog signaling. Nat Genet. 2006; 38(3): 303–311. [PubMed: 16493421]

Park TJ, Mitchell BJ, Abitua PB, Kintner C, Wallingford JB. Dishevelled controls apical docking and planar polarization of basal bodies in ciliated epithelial cells. Nat Genet. 2008; 40(7):871–879. [PubMed: 18552847]

Randlett O, Poggi L, Zolessi FR, Harris WA. The oriented emergence of axons from retinal ganglion cells is directed by laminin contact in vivo. Neuron. 2011; 70(2):266–280. [PubMed: 21521613]

Raymond PA, Barthel LK, Rounsifer ME, Sullivan SA, Knight JK. Expression of rod and cone visual pigments in goldfish and zebrafish: a rhodopsin-like gene is expressed in cones. Neuron. 1993; 10(6):1161–1174. [PubMed: 8318234]

Simons M, Mlodzik M. Planar cell polarity signaling: from fly development to human disease. Annu Rev Genet. 2008; 42:517–540. [PubMed: 18710302]

Stearns T, Evans L, Kirschner M. Gamma-tubulin is a highly conserved component of the centrosome. Cell. 1991; 65(5):825–836. [PubMed: 1840506]

Steinberg RH, Fisher SK, Anderson DH. Disc morphogenesis in vertebrate photoreceptors. J Comp Neurol. 1980; 190(3):501–508. [PubMed: 6771304]

Sugiyama Y, Stump RJ, Nguyen A, Wen L, Chen Y, Wang Y, Murdoch JN, Lovicu FJ, McAvoy JW. Secreted frizzled-related protein disrupts PCP in eye lens fiber cells that have polarised primary cilia. Dev Biol. 2010; 338(2):193–201. [PubMed: 19968984]

Vihtelic TS, Doro CJ, Hyde DR. Cloning and characterization of six zebrafish photoreceptor opsin cDNAs and immunolocalization of their corresponding proteins. Vis Neurosci. 1999; 16(3):571–585. [PubMed: 10349976]

Wallingford JB. Planar cell polarity signaling, cilia and polarized ciliary beating. Curr Opin Cell Biol. 2010; 22(5):597–604. [PubMed: 20817501]

Wallingford JB, Mitchell B. Strange as it may seem: the many links between Wnt signaling, planar cell polarity, and cilia. Genes Dev. 2011; 25(3):201–213. [PubMed: 21289065]

Wallingford JB, Rowning BA, Vogeli KM, Rothbacher U, Fraser SE, Harland RM. Dishevelled controls cell polarity during Xenopus gastrulation. Nature. 2000; 405(6782):81–85. [PubMed: 10811222]

Westerfield, M. The zebrafish book : a guide for the laboratory use of zebrafish (Brachydanio rerio). Eugene, OR: M. Westerfield; 1995.

Wolfrum U. Centrin in the photoreceptor cells of mammalian retinae. Cell Motil Cytoskeleton. 1995; 32(1):55–64. [PubMed: 8674134]

Yu X, Ng CP, Habacher H, Roy S. Foxj1 transcription factors are master regulators of the motile ciliogenic program. Nat Genet. 2008; 40(12):1445–1453. [PubMed: 19011630]

Zar, JH. Biostatistical analysis. Upper Saddle River, N.J: Prentice Hall; 1996.

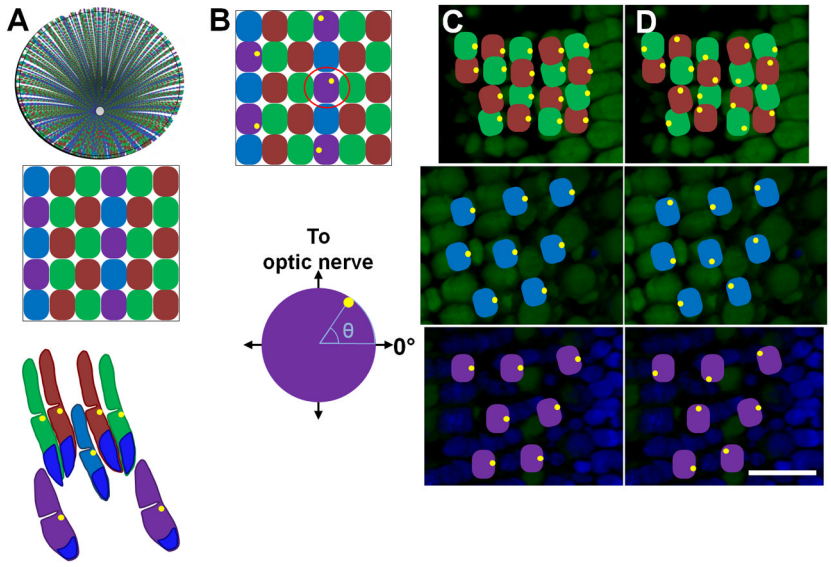

Figure 1. Basal body positioning within the zebrafish cone mosaic

(A) Top: Schematic of an adult retina showing the cone row mosaic radiating out from the optic nerve. Middle: Magnification (below) shows the mosaic pattern of the red- (R), green- (G), blue- (B), and UV- (U) sensitive cones. Bottom: Schematic of the vertical tiering of cones within the photoreceptor layer. Basal bodies (yellow dots) are located in the ellipsoids at the base of the outer segments. Nuclei are labeled in blue. (B) Top: Schematic with basal bodies in the UV-sensitive cones adopting a random distribution around the perimeter of the cell. Bottom: The angular position of a basal body in one selected UV-sensitive cone (below) is determined as shown. (C) Fluorescent image of an oblique cryosection through a retinal flatmount. Photoreceptor nuclei were stained with DAPI (blue). Autofluorescence (green) from excitation with 488 nm light shows inner and outer segments. (D–E) Potential basal body arrangements for red-/green-sensitive cones (top panels), blue-sensitive cones (middle panels), and UV-sensitive cones (bottom panels) at their appropriate depths in the retina are illustrated. Basal bodies may be asymmetrically polarized and similarly positioned or are randomly positioned at the apical end of the inner segment. Basal bodies are illustrated in yellow. Scale bar = 10 μm. Magenta-green copies are available in the Journal's supplemental data figures.

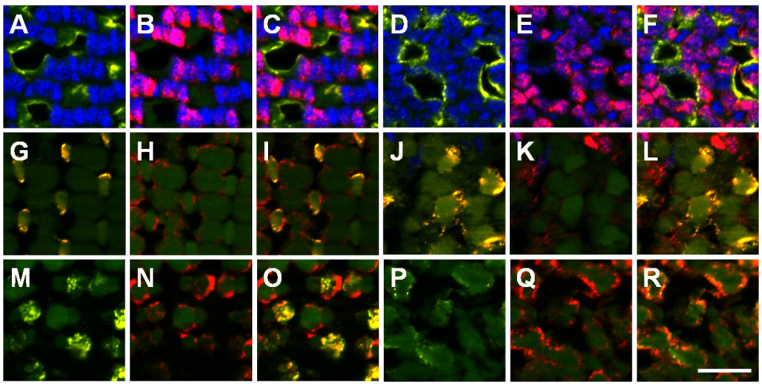

Figure 2.

Cone subtypes can be identified by the vertical tiering distribution. (A–F) UV opsin (yellow) marks UV-sensitive cones and Zpr-1 staining (red) marks the cell bodies of the red-/green-sensitive double cones in the adult mosaic (A,-C) and the larval retina (D–F) at the vertical location of the basal body. (G–L) Blue opsin (yellow) labels blue-sensitive cones and zpr-1 staining (red) labels red-/green-double cones in the adult mosaic (G–I) and the larval retina (J–L) at the vertical location of the basal bodies. (M–R) Green cone opsin (yellow) labels green-sensitive cones and colocalizes with one member of the double-cone pair labeled by Zpr-1 staining (red) in the adult mosaic (M–O) and the larval retina (P–R). Scale bar = 10 μm.

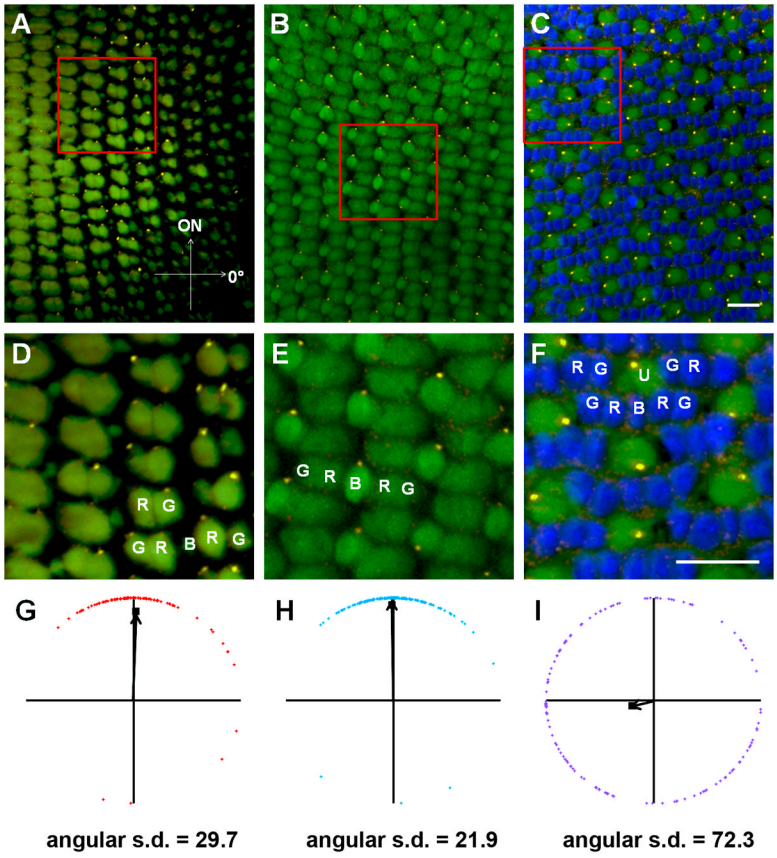

Figure 3.

Basal body positioning is strongly patterned in individual fields of red-/green- and blue-sensitive cones. (A–C) Sample portions of fields of cells at the depths of the basal bodies of (A) red-/green-sensitive cones, (B) blue-sensitive cones, and (C) UV-sensitive cones, along with their respective magnified subsets of cells (D–F),in adult light-adapted zebrafish retinas. γ-tubulin localized to basal bodies (yellow), while nuclei were counter-stained with DAPI (blue). Autofluorescence (green) from 488 nm excitation shows inner and outer segments. Some red-, green-, blue-, and UV-sensitive cones are labeled as R, G, B, and U, respectively. (G–I) Graphs of the positions of basal bodies from fields AC in which the positions of all the basal bodies of red-/green-, blue-, or UV-sensitive cones were plotted around a unit circle (red, blue, or purple diamonds, respectively), and the mean vector is indicated (black arrow). The angular position of each mean vector indicates the basal bodies' mean position around the periphery of the cell, and the distance of each mean vector from the origin indicates the strength of the trend. Optic nerve is up in all panels. Scale bars = 10 μm. Magenta-green copies are available in the Journal's supplemental data figures.

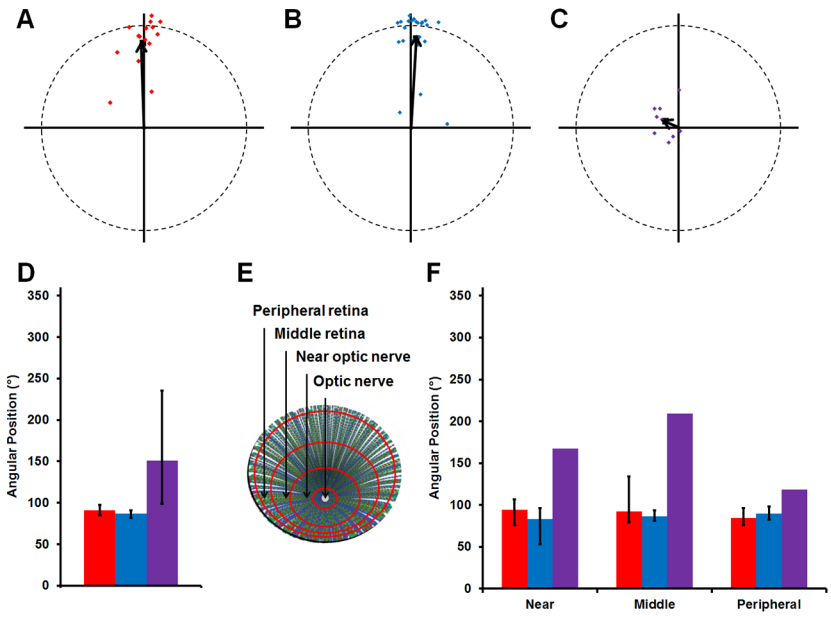

Figure 4.

Basal body positioning is consistent throughout the adult retina. (A–C) The mean vectors from individual fields of red-/green-, blue-, or UV-sensitive cone are plotted (red, blue, or purple diamonds, respectively). The grand mean vectors are also plotted (black arrows). Optic nerve is up. (D) The grand mean angular position of basal bodies is plotted for each subtype of cones. (E) Schematic of a flat-mounted retina showing the different regions where fields of cells were analyzed. (F) The mean position of basal bodies is shown for each subtype of cones in regions of the retina near the optic nerve, in the middle of the retina, and in the peripheral retina. Red-/green-, blue-, and UV-sensitive cones are shown in red, blue, and purple, respectively. Error bars represent the confidence intervals that are calculated to 95% confidence. The lack of error bars for UV-sensitive cones indicates the strength of the trend was too weak to calculate a confidence interval. Magenta-green copies are available in the Journal's supplemental data figures.

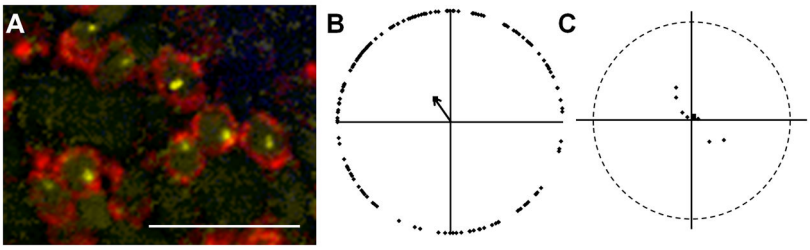

Figure 5.

Rod basal bodies are randomly positioned. (A) Basal bodies of rod photoreceptors within the mosaic of a dark-adapted retina. GFP immunoreactivity (red) labels rods in the XOPS-GFP line. γ-tubulin (yellow) localizes to basal bodies. Nuclei were stained with DAPI (blue). Autofluorescence at 488 nm (green) shows inner and outer segments. (B) Graphical analysis of rod basal bodies from an individual field of cells. The mean vector is indicated as a black arrow. (C) Plot showing the mean vectors from several individual fields of rods (small black diamonds) and the grand mean vector of these mean vectors (large black square). The optic nerve is up in all panels and all fields analyzed were from the middle or peripheral retina. Scale bars = 10 μm. Magenta-green copies are available in the Journal's supplemental data figures.

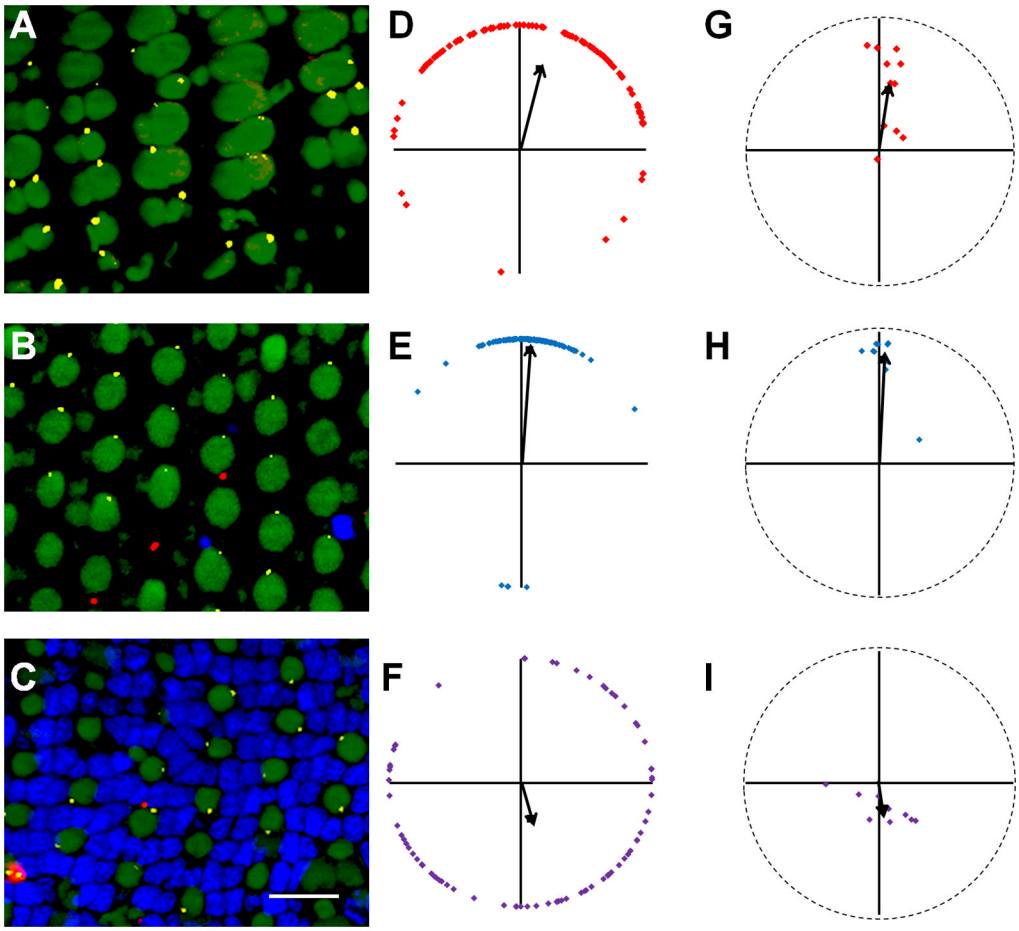

Figure 6.

Loss of rods does not affect basal body positioning in cones. Sample portions of fields of cells at the depths of the basal bodies of (A) red-/green-sensitive cones (B), blue-sensitive cones, and (C) UV-sensitive cones show basal body positioning in adult light-adapted XOPS-mCFP zebrafish retinas. (D–F) Shown are graphs of the positions of basal bodies from fields A–C in which the positions of all the basal bodies of red-/green-, blue-, or UV-sensitive cones were plotted around a unit circle (red, blue, or purple diamonds, respectively), and the mean vector is indicated (black arrow). (G–I) The mean vectors of basal bodies from individual fields of red-/green-, blue-, and UV-sensitive cones are plotted (red, blue, and purple diamonds, respectively). The grand mean vector of these mean vectors is indicated (black arrow). Optic nerve is up in all panels. Scale bar = 10 μm. Small numbers of remaining rods are occasionally visible (red). γ-tubulin (yellow) localizes to basal bodies. Nuclei were stained with DAPI (blue). Autofluorescence at 488 nm (green) shows inner and outer segments. All fields analyzed were from the middle retina.

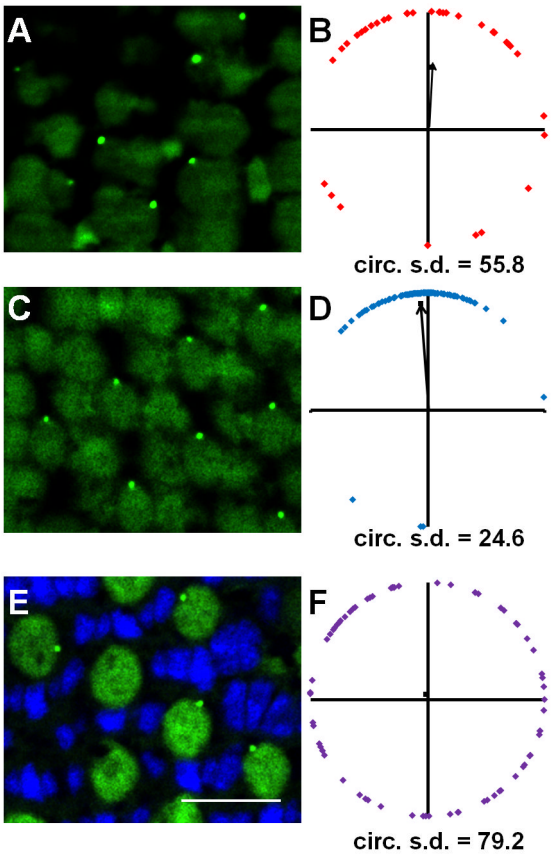

Figure 7.

Centrin-GFP labels basal bodies in the retinas of adult *Tg(XlRho:gap43-CFP)* transgenic zebrafish. (A, C, E) Sample portions of fields of cells at the depths of the basal bodies of (A) red-/green-sensitive cones, (C) blue-sensitive cones, and (E) UV-sensitive cones. GFP fluorescence localized to basal bodies (green), while nuclei were counter-stained with DAPI (blue). Autofluorescence (green) from 488 nm excitation shows inner and outer segments. (B, D, F) Graphs of the positions of basal bodies from fields A, C, E in which the positions of all the basal bodies of red-/green-, blue-, or UV-sensitive cones were plotted around a unit circle (red, blue, or purple diamonds, respectively), and the mean vector is indicated (black arrow). Optic nerve is up in all panels. Scale bars = 10 μm.

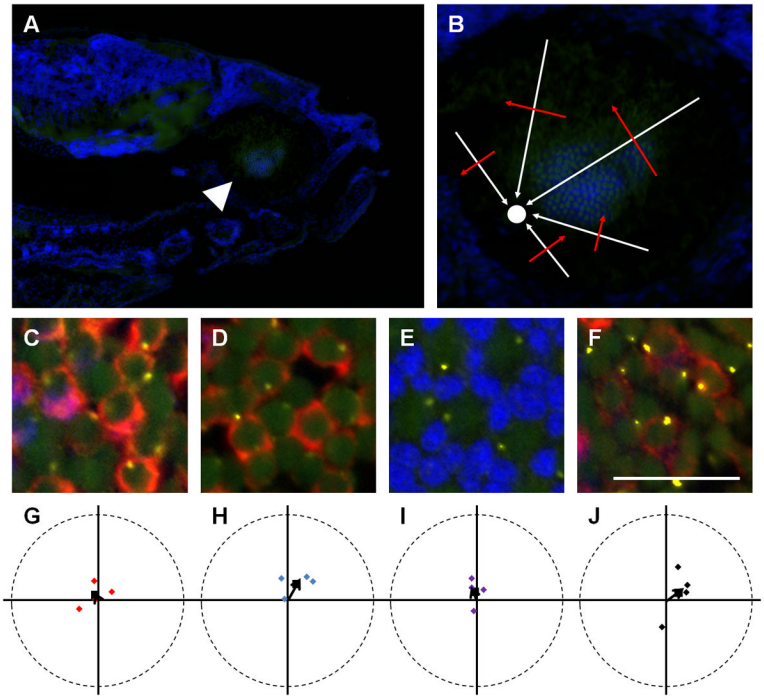

Figure 8.

Larval photoreceptor basal bodies are randomly positioned. (A) Sagittal section through a 7 dpf *Tg(-5actb2:cetn2-GFP)*^{cu6} larvae shows the optic nerve (arrowhead) and larval retinal mosaic. (B) Enlarged view of sectioned retina shows how to determine the orientation of cells relative to the optic nerve (white circle). White arrows indicate the direction of the optic nerve, while red arrows indicate the 90° perpendicular angle. (C–D) Immunostaining with Zpr-1 (red) and GFP antibodies (yellow) identifies basal bodies in red-/green-sensitive cones. Blue-sensitive cones were negative for Zpr-1 and 4c12 immunoreactivity (arrows). (E) Inner and outer segments (autofluorescence from excitation with 488 nm light) and basal bodies (yellow) of UV-sensitive cones. (F) Basal bodies (yellow) and 4C12 (red) immunopositive rods. (G–J) The mean angular positions of individual fields of red-/green-, blue-, and UV-sensitive cones and rods are plotted on circular graphs. Grand mean angular positions are shown as black squares. In all images, nuclei are counterstained with DAPI (blue). Scale bar = 10 μm (C–F). Magenta-green copies are available in the Journal's supplemental data figures

TABLE 1

Primary Antibodies

Antibody	Antigen	Dilution/species	Immunizing antigen	Source and catalog number
Gamma-tubulin	γ-tubulin	1:5000 Mouse, monoclonal	Synthetic peptide corresponding to amino acids 38-53 and conjugated to KLH	Sigma-Aldrich, St. Louis, MO Cat. No. T6557 Clone GTU-88
GFP	Green fluorescent protein (GFP)	1:500 Rabbit, polyclonal	Green fluorescent protein purified from *Aequorea Victoria*	Invitrogen, Life Technologies, Grand Island, NY Cat. No. A-111-22 Lot Nos. 1141866 and 632116
Green opsin	Zebrafish green opsin	1:200 Rabbit, polyclonal	C-terminal fragment	D. Hyde, University of Notre Dame, South Bend, IN, USA
Blue opsin	Zebrafish blue opsin	1:200 Rabbit, polyclonal	N-terminal fragment	D. Hyde, University of Notre Dame, South Bend, IN, USA
Ultraviolet opsin	Zebrafish ultraviolet opsin	1:200 Rabbit, polyclonal	N-terminal fragment	D. Hyde, University of Notre Dame, South Bend, IN, USA
Zpr-1	Arrestin 3-like	1:200 Mouse, monoclonal	Whole adult zebrafish retinal cells	Zebrafish International Resource Center (ZIRC), Eugene, OR. Cat. No. Zpr-1
4C12	Rod photoreceptors	1:150 Mouse, monoclonal	Whole zebrafish retina	J. Fadool, Florida State University, Tallahassee, FL, USA

TABLE 2

Numerical Analysis of Basal Body Position

Sample	Photoreceptor Subtype	Field Location	Mean Angular Position (0–360°)	95% Confidence Interval (°)	Circular Standard Deviation	Avg. # cells/field	# Fields	# Retinas	# Fish
Wild-type	Red/green	Near optic nerve	94	76–107	43.1	133	6	3	3
Wild-type		Middle retina	92	79–134	40.1	121	6	2	2
Wild-type		Peripheral retina	85	76–96	23.9	87	4	3	3
Wild type		Grand Mean	91	85–98	34.8	117	**Total = 16**	**4**	**3**
Wild-type	Blue	Near optic nerve	83	53–96	40.1	60	8	4	3
Wild-type		Middle retina	87	81–94	32.2	77	9	3	3
Wild-type		Peripheral retina	90	82–98	27.9	55	6	4	3
Wild-type		Grand Mean	87	82–91	32.5	65	**Total = 23**	**5**	**4**
Wild-type	UV	Near optic nerve	168	ND	73.9	72	3	3	2
Wild-type		Middle retina	209	ND	73.1	86	3	2	2
Wild-type		Peripheral retina	119	ND	74.5	63	3	3	2
Wild-type		Grand Mean	151	99–235	73.2	74	**Total = 9**	**5**	**4**
Wild-type	Rods	Middle and peripheral retina	58	ND	72.5	115	7	6	4
XOPS-mCFP	Red/green	Middle retina	81	58–91	56.3	119	11	6	3
XOPS-mCFP	Blue	Middle retina	88	76–95	34.0	78	10	6	3
XOPS-mCFP	UV	Middle retina	278	204–313	68.4	85	9	6	3
							Total = 30	**6**	**3**
Larvae (7 dpf)	Red/green	n/a	115	ND	74.5	66	4	4	4
Larvae (7 dpf)	Blue	n/a	60	ND	70.9	39	4	4	4
Larvae (7 dpf)	UV	n/a	100	ND	74.5	111	4	4	4
Larvae (7 dpf)	Rods	n/a	28	ND	68.1	34	4	4	4
							Total = 16	**9**	**9**